22nd AIAA International Communications Satellite Systems Conference & Exhibit 2004
9 - 12 May 2004, Monterey, California

AIAA 2004-3196

ANALYSIS AND SYNTHESIS OF ROTMAN LENSES

Peter S. Simon*
Space Systems/Loral, 3825 Fabian Way M/S G43, Palo Alto, CA 94303

Rotman lenses are attractive candidates for use in beam forming networks (BFNs) for satellite-based direct radiating arrays. This paper will review the basic design equations for a Rotman lens and will describe Rotman lens synthesis and analysis software developed by the author. The synthesis tool, named RLDESIGN, is written in MATLAB to automatically and rapidly solve the Rotman lens equations and interactively display the resulting lens geometry and performance parameters. It features a full graphical user interface customized to easily design, tune, and optimize a Rotman lens for a given application. The more rigorous analysis tool, named NARL (Numerical Analysis of Rotman Lens), is written in MATLAB and Fortran 95 and is based on a boundary integral/surface integral hybrid formulation. NARL uses a unique wide-band expansion of the parallel plate Green's function to enable rapid analysis of the lens for a large number of frequencies. To demonstrate the accuracy of the codes, comparisons are presented of the predictions of both RLDESIGN and NARL to measurements on a prototype Rotman lens.

Introduction

A Rotman lens[1] is a parallel-plate structure used as the beam forming network (BFN) for a linear array of radiating antenna elements. By stacking multiple lenses, one can form a BFN suitable for use with a planar array.[2] The advantages of Rotman lenses include monolithic construction, ease of manufacture, low cost, light weight, and simultaneous availability of many beams. Because it is a true time-delay device, the Rotman lens produces frequency-independent beam steering and is therefore capable of extremely wide-band operation. These features make the Rotman lens an attractive candidate for use in multibeam satellite-based applications.

Hansen[3,4] has presented compact formulas suitable for conveniently designing Rotman lenses, based on the simple ray theory of Rotman and Turner.[1] This theory is summarized and extended below, and a user-oriented design tool RLDESIGN that implements it is described.

Once an initial design has been generated, it is necessary to verify its performance with a more accurate analysis tool, one that can account for non-ideal factors such as multiple reflections within the parallel-plate region of the lens. Because of the large electrical area (typically hundreds of square wavelengths) occupied by a Rotman lens, a completely rigorous analysis is not feasible. The planar circuit approximation[5] applies to structures, like parallel-plate lenses, that are electrically thin in one dimension. It reduces the effort required for their analysis to that of solving a (line) integral equation for the relationship between the RF voltage and current at the periphery of the structure. This technique was first applied to the study of stripline and microstrip Rotman lenses by Chan,[6,7] and was subsequently also used by others for analysis of microstrip[8] and waveguide[9] Rotman lenses . In this work we describe the computer program NARL (Numerical Analysis of Rotman Lens) that also employs the planar circuit method to accommodate the presence of the large parallel-plate region. However, unlike previously reported efforts, we combine the planar circuit analysis with a full-wave, moment method (MoM) analysis of the individual tapered feed ports, using a novel, rigorous, polynomial representation of the stripline geometry potential Green's functions. By exploiting the frequency-independent nature of the polynomial coefficients, a large gain in numerical efficiency is obtained, sufficient to allow rigorous analysis of the tapered ports over the entire set of analysis frequencies.

The final section of this paper contains a comparison of the predictions of both RLDESIGN and NARL to measurements on a prototype Rotman lens.

Rotman Lens Synthesis Using RLDESIGN

Lens Design Equations

As shown in Fig. 1, a stripline Rotman lens consists of a parallel-plate region surrounded by N_a array ports, N_b beam ports, and some number of loaded dummy ports that are intended to provide a reflectionless termination of the parallel-plate region. Each array port is connected via a TEM cable of specified length to one radiating element of a linear antenna array. The lens designer begins by specifying the number of radiating elements N_a and their locations along the array axis, along with the number of beams N_b and the desired beam steering angles. The TEM cable lengths and the phase center locations

*Principal Engineer, RF Antenna Design Section, Antenna and Materials Technology Directorate.

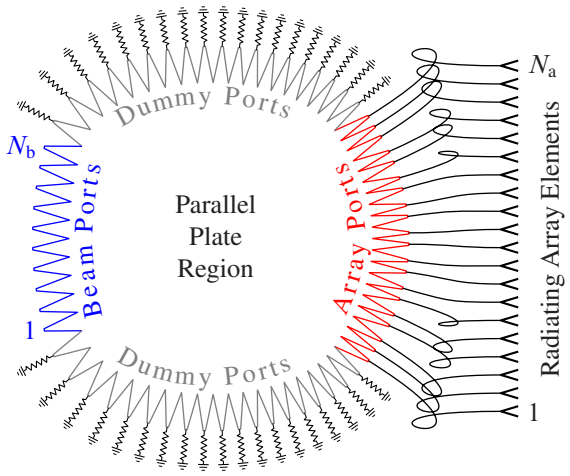

Fig. 1 Rotman Lens

for the array ports and beam ports (and thus the general shape of the parallel-plate region) are determined once the four basic Rotman lens parameters (α, β, f_1, and γ) are selected. These are defined with reference to Fig. 2, where it is seen that F_0, F_1, and F_2 are the three points ("foci") of the circular beam port arc for which there are no phase errors, f_1 is the (on-axis) focal length, f_2 is the off-axis focal length, ψ is the beam steering angle corresponding to the off-center focal point, y_3 is the location along the array axis of a typical radiating element, and w is the length of TEM cable connecting the element and its array port. The remaining lens parameters are the focal angle α, focal ratio $\beta = f_2/f_1$, and expansion factor $\gamma = \sin\psi/\sin\alpha$. As derived by Hansen,[3] the normalized length $W = w/f_1$ of the cable attached to the array element at $y = y_3$ satisfies the quadratic equation

$$aW^2 + bW + c = 0, \tag{1}$$

with coefficients a, b, and c defined by

$$a = 1 - \frac{(1-\beta)^2}{(1-\beta\cos\alpha)^2} - \frac{\zeta^2}{\beta^2}, \tag{2a}$$

$$b = -2 + \frac{2\zeta^2}{\beta} + \frac{2(1-\beta)}{1-\beta\cos\alpha} - \frac{\zeta^2\sin^2\alpha(1-\beta)}{(1-\beta\cos\alpha)^2}, \tag{2b}$$

$$c = -\zeta^2 + \frac{\zeta^2\sin^2\alpha}{1-\beta\cos\alpha} - \frac{\zeta^4\sin^4\alpha}{4(1-\beta\cos\alpha)^2} \tag{2c}$$

and with $\zeta = y_3\gamma/f_1$. A formula for the corresponding array port phase center location $P(x_2, y_2)$ was not provided by the previously cited references. However, it can be shown[10] that

$$X_2 \equiv \frac{x_2}{f_1} = 1 - \frac{\frac{1}{2}\zeta^2\sin^2\alpha + (1-\beta)W}{1-\beta\cos\alpha} \tag{3a}$$

$$Y_2 \equiv \frac{y_2}{f_1} = \zeta\left(1 - \frac{W}{\beta}\right). \tag{3b}$$

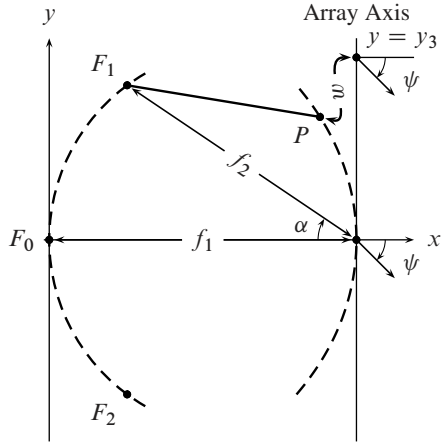

Fig. 2 Rotman lens parameters (after Hansen[3]).

It is also possible[10] to derive expressions for the beam port phase center coordinates (x_1, y_1) needed to steer the array to an angle θ:

$$X_1 \equiv \frac{x_1}{f_1} = \rho_0[1 - \cos(\alpha' + \phi)], \tag{4a}$$

$$Y_1 \equiv \frac{y_1}{f_1} = \rho_0\sin(\alpha' + \phi), \tag{4b}$$

where

$$\rho_0 = 1 - \frac{1-\beta^2}{2(1-\beta\cos\alpha)}, \tag{4c}$$

$$\alpha' = \mathrm{Sin}^{-1}\left(\frac{\sin\theta}{\gamma}\right), \tag{4d}$$

$$\phi = \mathrm{Sin}^{-1}\left(\frac{1-\rho_0}{\rho_0}\sin\alpha'\right). \tag{4e}$$

Approximate Lens Illumination Function

After the physical layout of the lens has been determined via the above equations, a prediction of the coupling between a typical beam port of width w_B and array port of width w_A is obtained using the approximate formula[11]

$$S_{AB} = j_0\left(\frac{kw_A}{2}\sin\phi_A\right) j_0\left(\frac{kw_B}{2}\sin\phi_B\right) \times \sqrt{\frac{w_A w_B}{\lambda d}}e^{-j(kd+\pi/4)}, \tag{5}$$

where $k = 2\pi/\lambda$ is the wavenumber in the dielectric substrate, d is the separation between port phase centers, $j_0(x) \equiv (\sin x)/x$, and ϕ_A and ϕ_B are the angles subtended about the phase centers, measured from the ports' boresight directions to the segment joining their phase centers, as shown in Fig. 3. Implicit in Eq. (5) is the assumption that the port apertures are uniformly illuminated. RLDESIGN uses this formula to provide predictions of illumination amplitude, phase error, and the resulting far-field array factor.

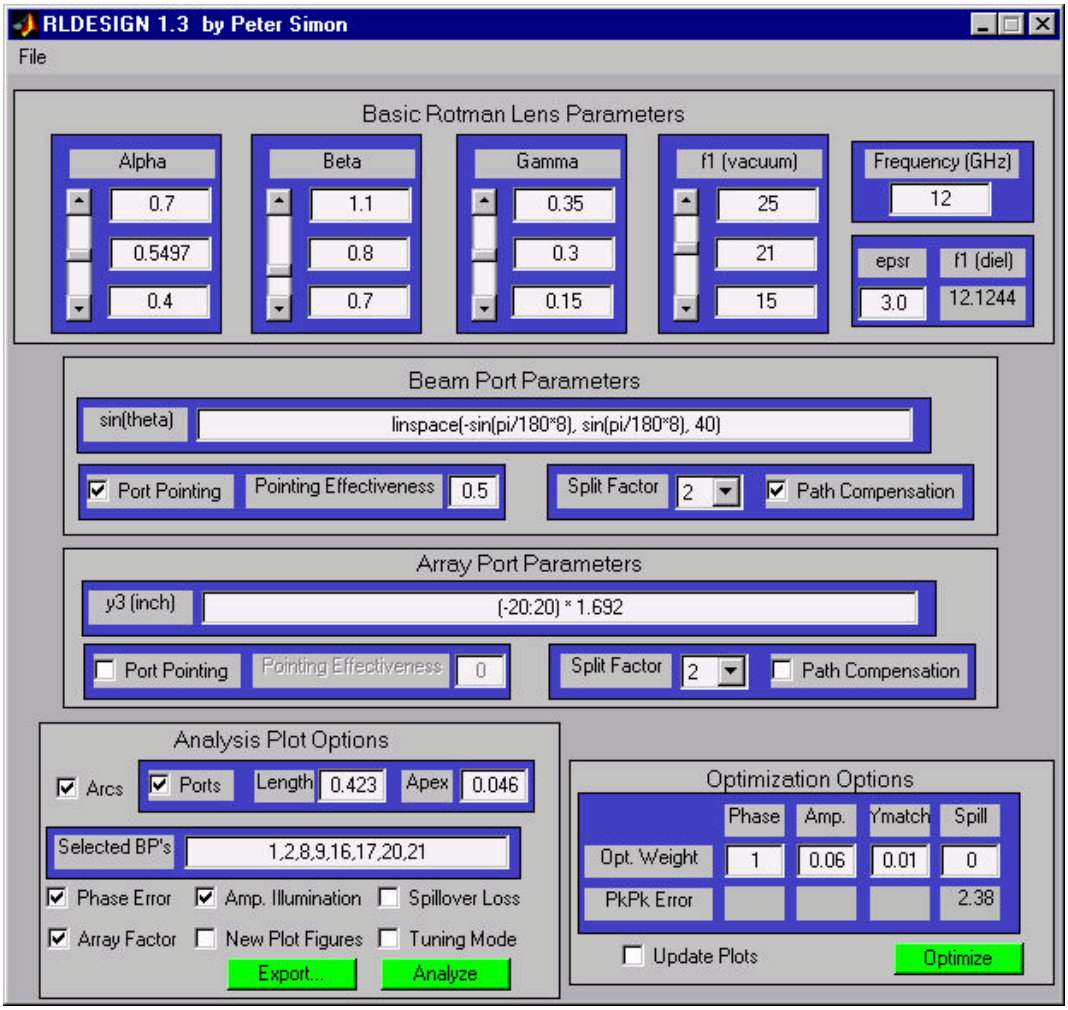

Fig. 4 The RLDESIGN main window.

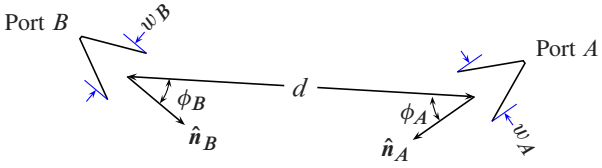

Fig. 3 Simple ray-based port coupling model.

RLDESIGN

The Rotman lens design equations have been incorporated into an intuitive design package named RLDESIGN. Implemented in MATLAB, RLDESIGN features a full graphic user interface (GUI), and facilitates rapid, interactive optimization of a Rotman lens for a particular application on PC platforms or Unix workstations. The main window for RLDESIGN is shown in Fig. 4, where it is seen that the GUI controls are grouped according to function. The various groups are discussed in the following paragraphs.

Basic Rotman Lens Parameters

Here the designer specifies the operating frequency and lens substrate permittivity, along with the four basic lens parameters α, β, γ, and f_1. Each of these four can be precisely set by typing a value into a field (the center edit box), or they can be continuously varied by adjusting a slider control between user-specified limits. RLDESIGN supports a so-called "tuning mode" wherein any adjustments made to these sliders result in immediate feedback in the form of updated lens contour plots and/or performance plots (discussed below). The slider limits (in the top and bottom edit boxes for each parameter) are also used as optimization variable bounds for the built-in optimizer.

Beam Port and Array Port Parameters

In the edit box labeled `sin(theta)` the user types an arbitrary MATLAB expression that evaluates to the sine of the desired steering angles. This method was chosen because frequently it is desired to specify a set

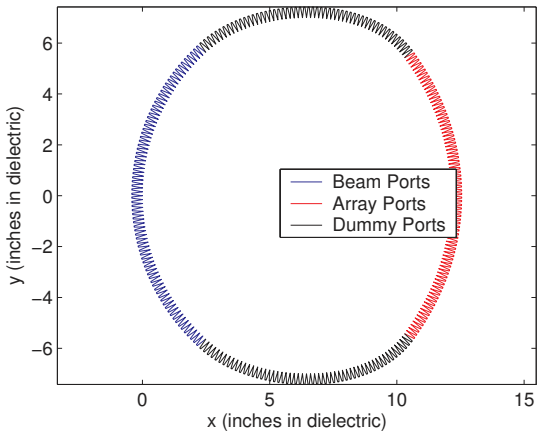

Fig. 5 Lens geometry generated by `Ports` checkbox.

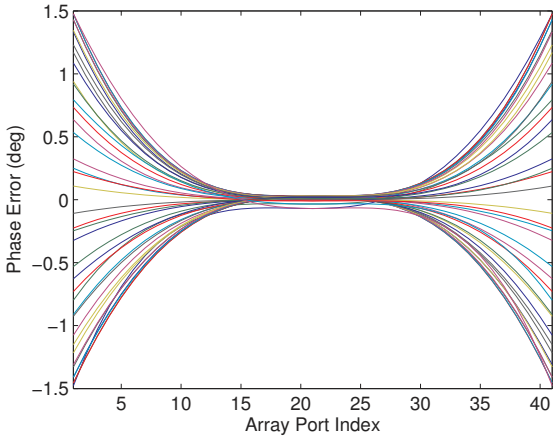

Fig. 6 Plot generated by `Phase Error` checkbox.

of steering angles that are uniformly distributed in sine space. For example, in Fig. 4 the MATLAB intrinsic function `linspace` has been used to request 40 beam ports steered to angles equally spaced in sine space, with end beams located at $\pm 8°$. Beam port phase center locations on the beam port arc are calculated from the steering angles using Eq. (4). The radiating array element locations are specified by a MATLAB vector expression typed by the user into the box labeled `y3 (inch)` as in Fig. 4 where 41 uniformly spaced elements are symmetrically disposed along the y axis with interelement spacing 1.692 in. The array port phase center locations are then obtained using Eq. (3).

The linearly tapered beam ports and array ports are by default oriented with their boresight normal to the arc on which they lie, but activating the `port pointing` checkbox causes them instead to be pointed to the center of the opposite arc. This can sometimes improve illumination symmetry and hence reduce spillover loss.

To achieve better lens illumination and port impedance match, it is often desirable to split each of the beam and/or array ports into two or more ports fed by an isolated Wilkinson power divider. RLDESIGN provides popup menus where the user can select a "split factor" of 1–4 to indicate how many such divisions should be applied to each port. The `path compensation` checkbox, when activated, instructs the program to adjust the simulated lengths of the lines feeding each arm of the Wilkinson divider to achieve equal path lengths to the center of the opposite arc.

Analysis Plot Options

These checkboxes are to select plots to be generated when the `Analyze` button is clicked. The `Arcs` option plots port phase center locations, while `Ports` draws the entire lens boundary, including array, beam, and dummy ports, as in Fig. 5. Various performance parameters can also be plotted, such as phase error (Fig. 6), amplitude illumination, and computed array factor (Fig. 7).

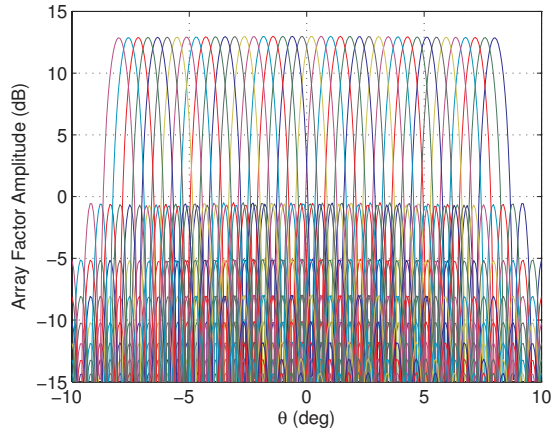

Fig. 7 Beam rosette generated by `Array Factor` checkbox.

Optimization Options

In addition to its manual tuning mode, RLDESIGN incorporates an automatic optimizer (based on the MATLAB Optimization Toolbox function `fminimax`) that attempts to adjust the four basic lens parameters so as to minimize an objective function consisting of a weighted sum of phase error, amplitude error, spillover loss, and "Ymatch." (The last quantity is a measure of the y-coordinate mismatch of the beam port and array port arc endpoints. Minimizing "Ymatch" allows for easier "clamming" of the lens boundary.) The user can specify the weighting to be applied to each component of the objective function, and a constant readout of the component values is provided during the optimization run, which typically takes only seconds. The user also has the option of viewing updated geometry and/or performance plots at each iteration.

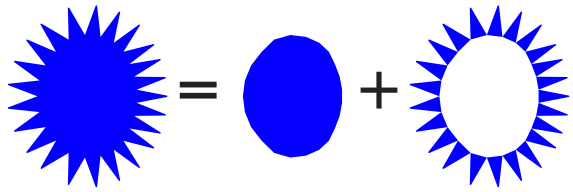

Fig. 8 NARL divides the analysis into two subproblems.

Rotman Lens Analysis Using NARL

Overview

Although RLDESIGN is extremely useful for synthesizing Rotman lens designs, it's simple physical optics/ray-tracing method is not capable of predicting several important performance parameters, including port return loss, neighboring port mutual coupling, and the ripple observed in the lens amplitude illumination due to reflections from imperfectly matched ports terminating the parallel plate region. A more accurate analysis method is needed to model these effects. Because of the large electrical area of the lens (typically hundreds of square wavelengths), analysis using completely rigorous methods such as the method of moments (MoM), finite elements (FE), or the finite difference time domain (FDTD) method is not feasible. Therefore, we adopt the same approach as previous workers, using the planar circuit method for the interior parallel-plate region, and combining its results with a separate analysis of the tapered feed ports. This decomposition is conceptually illustrated in Fig. 8.

Previous workers[6–8] have used an approximate equivalent waveguide model of the stripline or microstrip ports, involving the use of effective dimensions to account for fringing, along with an approximate tapered transmission line theory to account for higher mode reflections in the taper. Here, we avoid the use of effective dimensions by using a full-wave MoM solution for the ports that correctly accounts for fringing fields. The basis functions used here are the triangle subdomain functions of Rao, Wilton, and Glisson[12] (RWG) that can accommodate any polygonal port shape. We also employ a novel, wide-band formulation of the stripline potential Green's functions that makes the rigorous port analysis numerically efficient.

Parallel Plate Region

After temporarily removing the tapered feed ports from the stripline center conductor pattern of the lens, the remaining parallel plate region is just a convex polygon as shown in Fig. 8. Each polygon edge is referred to as a "port segment." To analyze this portion of the structure, Chan and others assumed a series of waveguide modes with sinusoidal transverse variation in each port segment. The original planar circuit formulation of Okoshi[5] assumed constant RF voltage and current density within each linear segment. Here we revert to Okoshi's original formulation, subdividing each port segment as necessary for sufficient accuracy, and noting that Okoshi's assumptions are completely consistent and compatible with the constant normal current density assumption for each edge in the RWG basis function formulation.

Following the reference[5] the open-circuit impedance matrix $\mathcal{Z}_{\text{pp}}$ for the parallel-plate region is found as $\mathcal{Z}_{\text{pp}} = \mathcal{U}^{-1}\mathcal{H}$, where

$$\mathcal{U}_{mn} = \begin{cases} -kW_n \cos\theta_{mn}\, H_1^{(2)}(kr_{mn}) & (m \neq n) \\ 2j & (m = n), \end{cases} \tag{6}$$

$$\mathcal{H}_{mn} = \begin{cases} \frac{j\omega\mu h}{2} H_0^{(2)}(kr_{mn}) & (m \neq n) \\ \frac{j\omega\mu h}{2}\left[1 - \frac{2j}{\pi}\left(\log\frac{kW_m}{4} - 1 + \gamma\right)\right] & (m = n), \end{cases} \tag{7}$$

$H_n^{(2)}$ is the Hankel function of the second kind of order n, W_m is the width of the mth segment, γ is Euler's constant, and r_{mn} and θ_{mn} are geometrical parameters.[5]

Feed Port Analysis

Wide-Band Green's Function

Each port is analyzed rigorously using a mixed-potential integral equation (MoM) and the RWG basis functions. The key feature that provides enough numerical efficiency to make this procedure feasible is the use of a wide-band Green's function for the potentials.

The structure for which the potential Green's functions are desired consists of a dielectric-loaded, parallel plate waveguide, bounded at $z = 0$ by a magnetic wall, at $z = h$ by an electric wall*, and unbounded as $\rho \to \infty$. We assume that the structure is electrically thin, so that

$$k_{\max} h \leq \frac{\pi}{4}, \tag{8}$$

where $k_{\max} = \omega_{\max}|\sqrt{\mu\epsilon}|$ is the magnitude of the wavenumber in the dielectric at the highest frequency of interest, μ and ϵ being the complex permeability and permittivity, respectively, of the dielectric substrate.

The magnetic vector potential Green's function G_x^A and electric scalar potential Green's function G^Φ are solutions to

$$(\nabla^2 + k^2)G_x^A(\boldsymbol{r}) = -\mu\delta(\boldsymbol{r}), \tag{9a}$$

$$(\nabla^2 + k^2)G^\Phi(\boldsymbol{r}) = -\frac{1}{\epsilon}\delta(\boldsymbol{r}), \tag{9b}$$

where $k = \omega\sqrt{\mu\epsilon}$ is the dielectric wavenumber, $\boldsymbol{\rho} = x\hat{\boldsymbol{x}} + y\hat{\boldsymbol{y}}$, and $\boldsymbol{r} = \boldsymbol{\rho} + z\hat{\boldsymbol{z}}$, and we have exploited

*The sources are limited to the plane $z = 0$ so that the symmetry of the resulting fields allows us to restrict consideration to only half ($0 < z < h$) of the full structure.

the translational invariance of the structure to place the sources at the origin. The Green's functions are subject to the boundary conditions

$$G_x^A(x,y,h) = G^\Phi(x,y,h) = 0, \tag{10a}$$

$$\frac{\partial G_x^A}{\partial z}(x,y,0) = \frac{\partial G^\Phi}{\partial z}(x,y,0) = 0, \tag{10b}$$

and the radiation condition as $\rho \to \infty$. Since these two functions satisfy identical boundary conditions and the same partial differential equation (up to a constant), they are equal within a constant multiplier. Therefore, we will seek only the Green's function G that satisfies

$$(\nabla^2 + k^2)G(\boldsymbol{r}) = -\delta(\boldsymbol{r}), \tag{11}$$

subject to the same boundary conditions. For use in the MoM procedure we only require this function to be evaluated in the plane $z = 0$. In this case $G(\boldsymbol{r})|_{z=0} = G(\boldsymbol{\rho}) = G(\rho)$, since there is no angular dependence.

We will make use of previously derived formulas for a rectangular, stripline cavity[13] to find this desired Green's function. Adjusting notation for the different orientation of the coordinate system, and allowing the cavity walls to recede to infinity, we find that G can be expressed with negligible error as a polynomial in k:

$$G(\rho) = \frac{1}{\pi h}\sum_{q=0}^{2}\frac{a_q}{q!}\left(\frac{k}{k_{\max}}\right)^{2q}\left(\frac{k_{\max}\rho}{2}\right)^{q} \times \times \sum_{n=0}^{\infty}\left(\frac{k_{\max}}{k_{yn}}\right)^{q} K_q(k_{yn}\rho) \tag{12}$$

where $k_{yn} = (n + 1/2)\pi/h$, K_q is the modified Bessel function (MacDonald's function) of order q, $a_0 = 1$, and a_1 and a_2 are constants chosen to minimize the maximum error in the approximation $\frac{1}{1-x} \approx 1 + a_1 x + a_2 x^2$ for $0 \le x \le \frac{k_{\max}}{k_{y0}}$. We note that (8) is equivalent to the condition that $k_{\max}/k_{y0} \le 1/2$. Equation (12) is very useful for moderate to large values of ρ due to the rapid, exponential decay of the modified Bessel function, and because of the fact that (12) is in the form of a polynomial in k^2. However, for $\rho < h/2$ the sum over n in (12) is slowly convergent and actually diverges as $\rho \to 0$. This behavior is not unexpected, since the potentials must exhibit a singularity proportional to $1/\rho$ at $\rho = 0$.

An alternative, quasi-static series for G that is useful for small arguments was derived using the Poisson summation formula[13] and is presented below, specialized to the case where source and observation points are restricted to the $z = 0$ plane:

$$G(\rho) = \frac{1}{\pi h}\sum_{q=0}^{2}\frac{a_q}{q!2^q}\left(\frac{k}{k_{\max}}\right)^{2q} S_q(\rho) \tag{13}$$

where

$$S_0(\rho) = \frac{1}{2\tilde{\rho}} + \sum_{n=1}^{\infty}\frac{(-1)^n}{r_n} \tag{14a}$$

$$S_1(\rho) = \frac{1}{2}(k_{\max}h)^2\left[1 - \tilde{\rho} - 2\sum_{n=1}^{\infty}(-1)^n X_n\right], \tag{14b}$$

$$S_2(\rho) = \frac{1}{2}(k_{\max}h)^4\left[\frac{2}{3} - \frac{1}{2}\tilde{\rho}^2 + \frac{1}{3}\tilde{\rho}^3 + \sum_{n=1}^{\infty}(-1)^n\left(\frac{2}{3}X_n^3 + 4nX_n^2 + 8n^2 W_n\right)\right] \tag{14c}$$

and we have defined $\tilde{\rho} = \rho/h$, $r_n = \sqrt{\tilde{\rho}^2 + 4n^2}$, $X_n = r_n - 2n$, $W_n = X_n - \frac{\tilde{\rho}^2}{4n}$.

The series in (14) require acceleration before they can be efficiently evaluated. To accomplish this, each summand is expanded in a Maclaurin series in the variable $1/n$ to determine its asymptotic behavior. The asymptotic terms are then subtracted termwise from the summand and added back in after being summed in closed form (a so-called "Kummer's transformation"). The result is

$$S_0(\rho) = \frac{1}{2\tilde{\rho}} - \frac{C_1}{2} + \frac{C_3\tilde{\rho}^2}{16} + \sum_{n=1}^{\infty}(-1)^n\left(\frac{1}{r_n} - \frac{1}{2n} + \frac{\tilde{\rho}^2}{16n^3}\right) \tag{15a}$$

$$S_1(\rho) = (k_{\max}h)^2\left\{\frac{1-\tilde{\rho}}{2} + \frac{C_1\tilde{\rho}^2}{4} - \frac{C_3\tilde{\rho}^4}{64} - \sum_{n=1}^{\infty}(-1)^n\left[X_n - \frac{\tilde{\rho}^2}{4n} + \frac{\tilde{\rho}^4}{64n^3}\right]\right\} \tag{15b}$$

$$S_2(\rho) = \frac{(k_{\max}h)^4}{2} \times \left(\frac{2}{3} - \frac{\tilde{\rho}^2}{2} + \frac{\tilde{\rho}^3}{3} + \frac{1}{3}S_{21} + 2S_{22} + 4S_{23}\right) \tag{15c}$$

where the auxiliary series are

$$S_{21} = -\frac{C_3\tilde{\rho}^6}{32} + \sum_{n=1}^{\infty}(-1)^n\left[2X_n^3 - \frac{\tilde{\rho}^6}{32n^3}\right], \tag{16a}$$

$$S_{22} = -\frac{\tilde{\rho}^4 C_1}{8} + \frac{\tilde{\rho}^6 C_3}{64} + \sum_{n=1}^{\infty}(-1)^n\left[2nX_n^2 - \frac{\tilde{\rho}^4}{8n} + \frac{\tilde{\rho}^6}{64n^3}\right] \tag{16b}$$

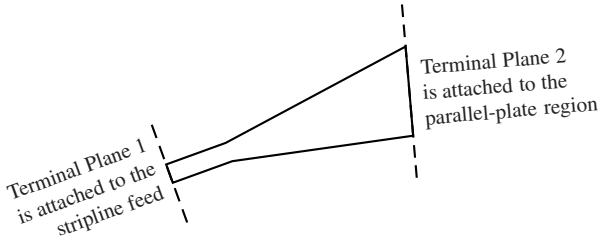

Fig. 9 A typical tapered feed port.

$$S_{23} = \frac{\tilde{\rho}^4 C_1}{32} - \frac{\tilde{\rho}^6 C_3}{256} + \sum_{n=1}^{\infty} (-1)^n \left[2n^2 X_n - \frac{\tilde{\rho}^2 n}{2} + \frac{\tilde{\rho}^4}{32n} - \frac{\tilde{\rho}^6}{256 n^3} \right] \tag{16c}$$

and

$$C_1 = \sum_{n=1}^{\infty} \frac{(-1)^{n+1}}{n} = \ln(2) \tag{17a}$$

$$C_3 = \sum_{n=1}^{\infty} \frac{(-1)^{n+1}}{n^3} = 0.9015426773696957\ldots \tag{17b}$$

Following the acceleration procedure all of the summands in (15) and (16) now decay as n^{-5}, so that the series converge quite rapidly. The series in (17) are related to the Riemann zeta function and are tabulated.[14]

Moment Method Formulation

The MoM formulation generally follows that of the original reference[12] except for a few modifications. First, the definition of the basis function used here does not include the length of the defining edge as a factor. This change means that the basis function coefficients $\{I_n\}$ now have units of current, and their interpretation is that I_n is the total current crossing the nth edge of the triangulated surface. It follows that the generalized impedance matrix $\mathcal{Z}$ arising from the MoM formulation has units of impedance, a physically appealing and useful outcome.

Second, unlike in the original RWG formulation, basis functions are defined for some of the edges located on the boundary of the port. The support of such basis functions is limited to the single adjacent triangle, rather than a pair of adjacent triangles as for an interior edge. The geometry of a typical feed port is shown in Fig. 9. It consists of a polygonal region in the x-y plane. The tapered feed port is attached at its narrow end to a uniform-width strip transmission line, and at the wide end it is connected to the Rotman lens parallel-plate region. The surface of the port is tessellated using triangles, resulting in N_1 and N_2 triangle edges along the port terminal planes at the narrow and wide ends, respectively. These correspond to N_1 and N_2 ports of the structure's equivalent circuit. The goal of the MoM analysis is to determine the open-circuit impedance matrix $\mathcal{Z}^{\text{oc}}$ that characterizes the $(N_1 + N_2)$-port equivalent circuit of the tapered feed port. As a first step, the MoM analysis is used to find the generalized impedance matrix $\mathcal{Z} \in \mathbb{C}^{N \times N}$ of the structure, where N is the total number of electric current basis functions. Once $\mathcal{Z}$ has been determined, $\mathcal{Z}^{\text{oc}}$ is obtained using the formula

$$\mathcal{Z}^{\text{oc}} = \mathcal{Z}_{11} - \mathcal{Z}_{12} \mathcal{Z}_{22}^{-1} \mathcal{Z}_{21} \tag{18}$$

where

$$\mathcal{Z} = \begin{bmatrix} \mathcal{Z}_{11} & \mathcal{Z}_{12} \\ \mathcal{Z}_{21} & \mathcal{Z}_{22} \end{bmatrix} \tag{19}$$

has been partitioned assuming that the first block of $N_1 + N_2$ unknowns corresponds to edges at the two terminal planes. Thus, $\mathcal{Z}_{11}$ is a square matrix of dimension $N_1 + N_2$, $\mathcal{Z}_{12}$ has dimensions $(N_1+N_2)\times(N-N_1-N_2)$, etc. To maintain consistency with standard conventions for electrical networks it is necessary that the basis functions associated with the port terminal planes be oriented to define positive current flow *into* the port.

Finally, because of the special form used for the potential Green's functions, the integrals needed to compute $\mathcal{Z}$ are also expressed as polynomials in frequency. Their coefficients are computed only a single time, then stored in matrices for reuse at each desired analysis frequency. This reduces the effort needed to compute the contributions to $\mathcal{Z}$ (for the second and subsequent analysis frequencies) to mere polynomial evaluation. For multi-frequency analysis we realize a drastic reduction in matrix fill time, which dominates total execution time for the MoM procedure. For maximum efficiency the MoM portion has been coded in Fortran 95. CPU time requirements for some numerical examples are given later in this paper.

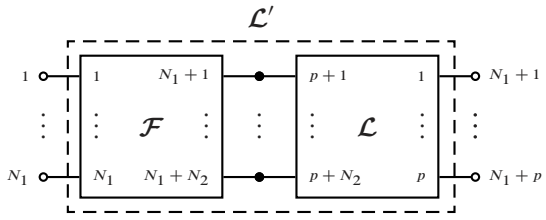

Fig. 10 Interconnection of feed port and lens networks.

Network Interconnection

Having determined the impedance matrices for the parallel-plate region and feed ports, it is necessary to combine them appropriately to find the matrix of the complete lens network. Each feed port in turn is attached to the composite lens network in an iterative procedure, one typical stage of which is illustrated in Fig. 10. As shown there, the partially combined lens network $\mathcal{L}$ contains $p + N_2$ ports, of which the last N_2 are to be connected to the last N_2 ports of the feed network $\mathcal{F}$. The resulting $(p + N_1)$-port network $= \mathcal{L}'$ is then ready to

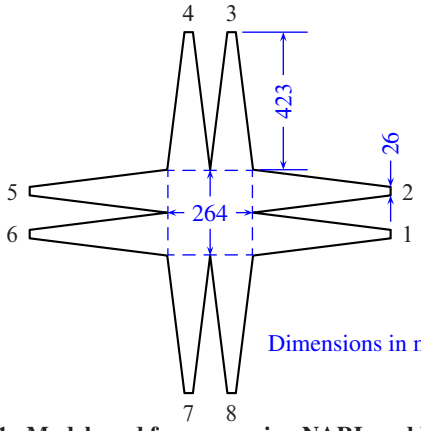

Fig. 11 Model used for comparing NARL and IE3D.

be combined with the next feed network. The formula for $\mathcal{L}'$ in terms of $\mathcal{F}$ and $\mathcal{L}$ is derived using techniques similar to those used for scattering matrices with the multiport connection method.[15] After partitioning the $\mathcal{F}$ and $\mathcal{L}$ matrices, the interconnection condition of equal voltages and opposite currents is enforced for each pair of terminals to be connected. The final result can be expressed most concisely in MATLAB notation as follows:

```
L = ...
 blkdiag(F(1:N1, 1:N1), L(1:p, 1:p)) + ...
 [F(1:N1, N1+1:N1+N2);-L(1:p, p+1:p+N2)] * ...
 ((F(N1+1:N1+N2, N1+1:N1+N2) + ...
   L(p+1:p+N2, p+1:p+N2)) \ ...
   [-F(N1+1:N1+N2, 1:N1), L(p+1:p+N2, 1:p)]);
```

After all feed ports have been connected, the impedance matrix is converted to a scattering matrix, which may then be further combined with the scattering matrices of the Wilkinson power dividers used to feed pairs of ports. The final, reduced scattering matrix provides all quantities of interest to the lens designer.

Code Validation

NARL Versus IE3D Test Case

As a preliminary test the small Rotman lens-like structure shown in Fig. 11 was analyzed using both NARL and IE3D, a commercial MoM tool. The substrate was taken to be Duroid 6002 ($\epsilon_r = 2.94$, $\tan\delta = 0.0015$) with ground plane spacing 43 mil. The structure was analyzed at 111 equally spaced frequencies from 1 to 12 GHz. For IE3D, a $\lambda/20$ mesh (at the highest frequency) was used, with edge cells enabled for higher accuracy, and with the fast sweep algorithm enabled. This resulted in a full analysis performed at 13 frequencies and interpolation at the remaining 98 frequencies. The IE3D run required 3 hr on a 2.4 GHz Pentium 4 machine. The NARL runs were performed on a 500 MHz Pentium 3 for maximum edge lengths of $\lambda/10$, $\lambda/20$, $\lambda/30$, and $\lambda/40$. These same 111 frequencies required 16 sec, 32 sec, 118 sec, and 257 sec, respectively; all a small fraction of the time needed for IE3D.

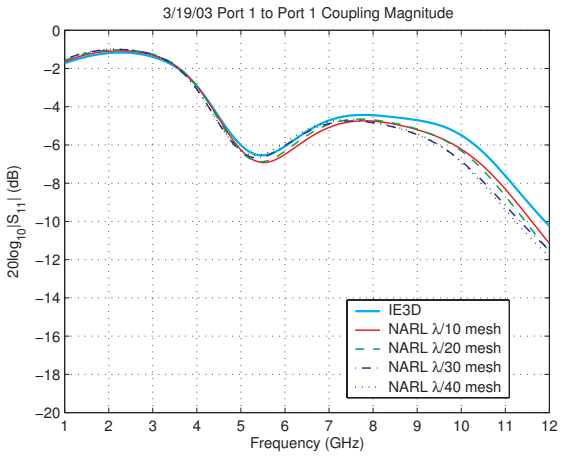

Fig. 12 NARL vs. IE3D port 1 reflection magnitude.

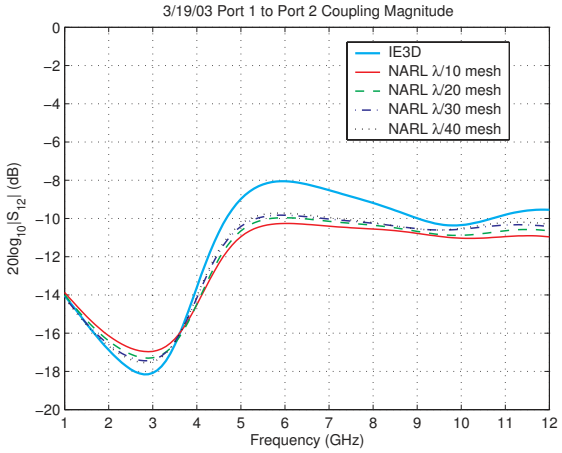

Fig. 13 NARL vs. IE3D ports 1–2 coupling magnitude.

Comparisons of return loss and port coupling magnitude are shown in Figs. 12–14, where the agreement is seen to be generally very good over the 12:1 frequency band, although it is slightly worse for the mutual coupling between ports 1 and 2. This can be understood by realizing that the direct electromagnetic coupling that exists between neighboring edges of adjacent feed ports is correctly accounted for by the full-wave analysis of IE3D but is ignored by NARL.

Comparison to Prototype Lens Measurements

Scattering parameter measurements using an automated network analyzer were taken on a prototype stripline Rotman lens developed under an internal research and development program. The lens, as shown in Figs. 15 and 16, has $N_a = 41$ array ports and $N_b = 46$ beam ports, and is constructed from Duroid 6002 with 43 mil ground plane spacing. It is intended to scan to $\pm 8°$, suitable for use on a satellite in geosynchronous orbit. The measured data was compared to predictions of the RLDESIGN and NARL codes.

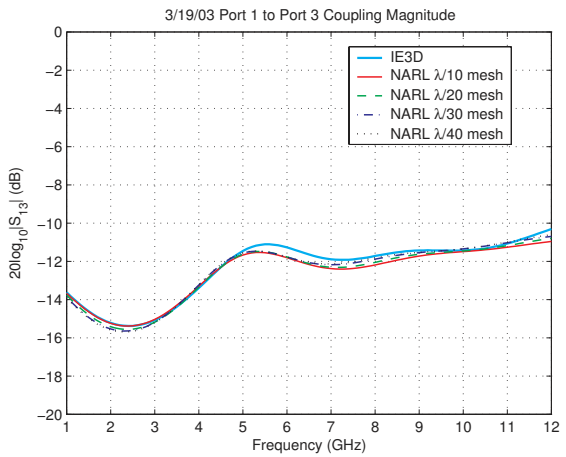

Fig. 14 NARL vs. IE3D ports 1–3 coupling magnitude.

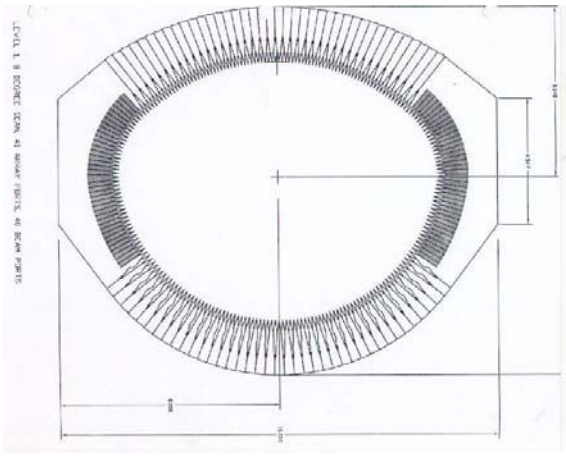

Fig. 15 Center conductor pattern of prototype lens.

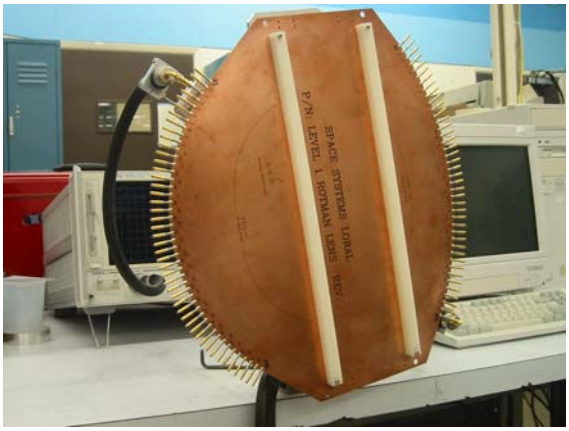

Fig. 16 Network analyzer measurement of prototype lens.

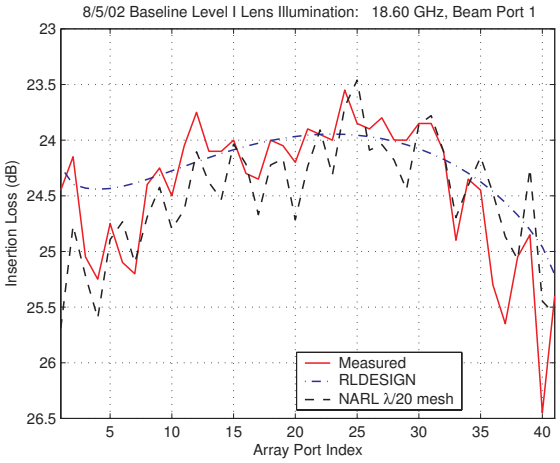

Fig. 17 Illumination amplitude for end beam port.

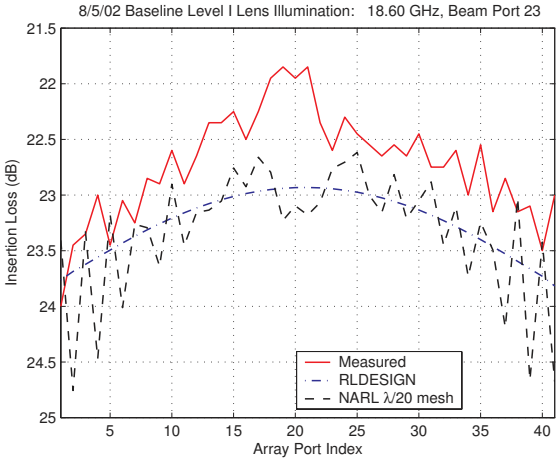

Fig. 18 Illumination amplitude for a central beam port.

Illumination amplitude for beam port 1 at 18.6 GHz is shown in Fig. 17. Ripple due to multiple reflections within the parallel plate region is clearly evident in the measured data and NARL prediction. The quality of agreement between these two is remarkable, especially considering the fact that both measured and predicted data include the effects of the Wilkinson power dividers feeding the split ports on both sides of the lens. A similar comparison for a central beam port is shown in Fig. 18, where the agreement is not as good. Both NARL and RLDESIGN appear to be overestimating the loss by approximately $1/2$ dB for this near-center beam port.

Fig. 19 provides a comparison of measured and predicted array pattern rosettes at 20 GHz for beams 1–24, normalized to a peak value of 0 dB. The agreement with measured data appears to be good for both RLDESIGN and NARL. A magnified view of the end beams is shown in Fig. 20 where a rolloff is observed in the beam peak gains. It is seen that NARL is able to predict the rolloff more accurately than RLDESIGN.

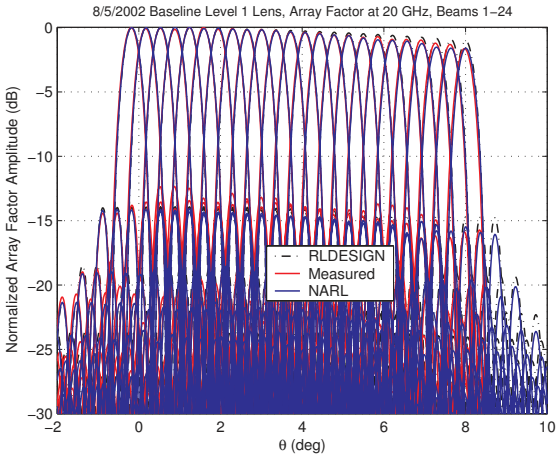

Fig. 19 Array factor rosette, beams 1–24.

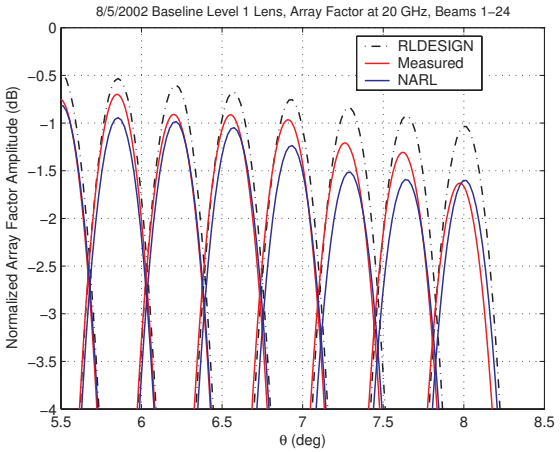

Fig. 20 Array factor rosette, end beams.

A return loss comparison for beam port 19 is presented in Fig. 21. These results are typical, in that NARL predicts a dip in the return loss that is not seen in the measured data. It is thought that this discrepancy may be due to some error in modeling (or manufacturing) the Wilkinson power dividers, especially considering the excellent correlation that was achieved with the IE3D model.

Figs. 22 and 23 show the comparisons of predicted and measured mutual coupling between neighboring beam ports and beam ports separated by three intervening ports. Good agreement between predictions and measurements is observed.

The NARL calculations for the prototype lens were performed on a Digital Alpha DS20E workstation using both a $\lambda/10$ and $\lambda/20$ mesh size. The lens was analyzed at 81 equally spaced frequencies between 18 GHz and 22 GHz. A breakdown of the CPU time needed for the analysis is shown in Table 1.

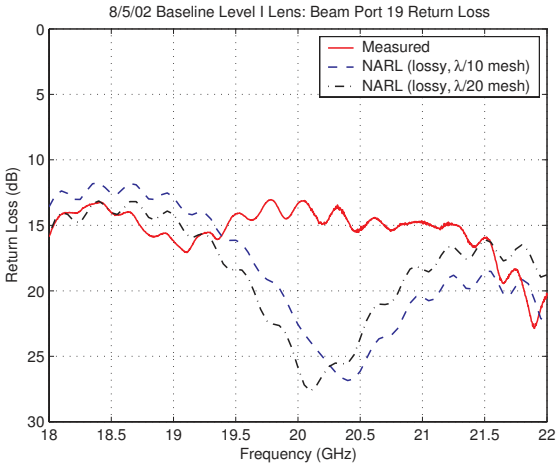

Fig. 21 Beam port 19 return loss.

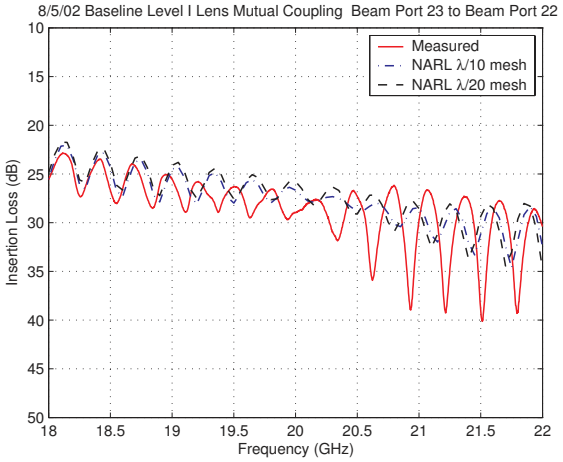

Fig. 22 Measured and calculated mutual coupling between beam ports 23 and 22.

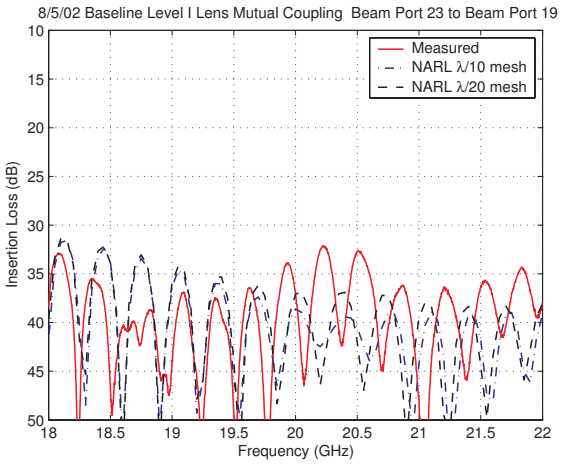

Fig. 23 Measured and calculated mutual coupling between beam ports 23 and 19.

Max. segment length	$\lambda/10$	$\lambda/20$
# Ports to Analyze	281	281
# Par. Plate Boundary Segments	1352	2573
Port Analysis CPU min.	17	183
PP Region CPU min.	47	386
Linear algebra CPU min.	83	690
Total CPU min.	147	1259
Avg. CPU min/freq.	2	16

Table 1 CPU time for NARL analysis of prototype lens.

Conclusions

The design equations for Rotman lenses were reviewed and new equations for locating the beam ports and array ports were presented. A powerful interactive tool, RLDESIGN, was developed that solves the lens equations and allows rapid optimization of a lens design for a given application. RLDESIGN is based on a simple ray-optical analysis, yet provides much useful information on lens performance including amplitude illumination, phase error, spillover loss, array factor patterns, and lens geometry. The latter can easily be exported to a CAD program for detailed layout. RLDESIGN will automatically add tapered beam ports, array ports, and dummy ports to the lens periphery, and it allows for split ports fed with Wilkinson power dividers.

A more rigorous analysis tool, NARL, was also developed to provide more accurate and detailed information about the lens performance. It combines the planar circuit method with a novel, wide-band, full-wave analysis of the tapered feed ports, resulting in a numerically efficient and accurate analysis that provides the full scattering matrix of the $(N_a + N_b)$-port lens, including the effects of multiple reflections. From the scattering matrix one can obtain all the outputs available from RLDESIGN in addition to other important performance parameters such as as port match, mutual coupling, and lens illumination ripple. NARL was validated by comparing its predictions on a small lens-like stripline structure to those of a commercial electromagnetic simulator program.

Both NARL and RLDESIGN were validated by comparing their predictions to measurements made on a prototype Rotman lens having 41 array ports and 46 beam ports.

References

[1]Rotman, W. and Turner, R., "Wide-angle microwave lens for line source applications," *IEEE Trans. Antennas Propagat.*, Vol. AP-11, No. 6, Nov. 1963, pp. 623–632.

[2]Chan, K. K. and Rao, S. K., "Design of a Rotman lens feed network to generate a hexagonal lattice of multiple beams," *IEEE Trans. Antennas Propagat.*, Vol. 50, No. 8, Aug. 2002, pp. 1099–1108.

[3]Hansen, R. C., "Design trades for Rotman lenses," *IEEE Trans. Antennas Propagat.*, Vol. 39, No. 4, Apr. 1991, pp. 464–472.

[4]Hansen, R. C., *Phased Array Antennas*, Wiley, 1998.

[5]Okoshi, T. and Miyoshi, T., "The planar circuit—An approach to microwave integrated circuitry," *IEEE Trans. Microwave Theory Tech.*, Vol. MTT-20, No. 4, Apr. 1972, pp. 245–252.

[6]Chan, K. K., "Field analysis of planar bootlace lens feeds," *Proc. Int. Conf. Radar*, Paris, France, Apr. 1989, pp. 273–278.

[7]Chan, K. K., "Planar waveguide model of Rotman lens," *Proc. IEEE Antennas and Propagat. Int. Symp. Dig.*, Vol. 2, San Jose, CA, June 1989, pp. 651–654.

[8]Peterson, A. F. and Rausch, E. O., "Validation of integral equation model with high-dielectric microstrip Rotman lens measurements," *Proc. 1991 Antenna Applications Symp.*, University of Illinois, Monticello, IL, Sept. 1991.

[9]Peterson, A. F. and Rausch, E. O., "Scattering matrix integral equation analysis for the design of a waveguide Rotman lens," *IEEE Trans. Antennas Propagat.*, Vol. 47, No. 5, May 1999, pp. 870–878.

[10]Simon, P. S., "Formulas for Rotman lens design," Memorandum AAS-02-0004, Space Systems/Loral, January 31 2002.

[11]Simon, P. S., "Reciprocity derivation of Rotman lens S-parameters," Memorandum AAS-03-0038, Space Systems/Loral, 24 October 2003.

[12]Rao, S. M., Wilton, D. R., and Glisson, A. W., "Electromagnetic scattering by surfaces of arbitrary shape," *IEEE Trans. Antennas Propagat.*, Vol. AP-30, No. 3, May 1982, pp. 409–418.

[13]Richards, W. F., McInturff, K., and Simon, P. S., "An efficient technique for computing the potential Green's functions for a thin, periodically excited parallel plate waveguide bounded by electric and magnetic walls," *IEEE Trans. Microwave Theory Tech.*, Vol. MTT-35, No. 3, Mar. 1987, pp. 276–281.

[14]Abramowitz, M. and Stegun, I. A., editors, *Handbook of Mathematical Functions*, Dover Publications, Inc., 1972.

[15]Gupta, K. C., Garg, R., and Chadha, R., *Computer-Aided Design of Microwave Circuits*, Artech House, Dedham, MA, 1981.